

Thermal-hydraulic performance of mist/compressed humid air two-phase flow in an airfoil channel recuperator

Junlin Chen^{a,c,e}, Jiangfeng Guo^{a,b,c,d*}, Xunfeng Li^{a,b,c}, Xiulan Huai^{a,b,c*}, Keyong Cheng^{a,b,c}

^aInstitute of Engineering Thermophysics, Chinese Academy of Sciences, Beijing 100190, China

^bUniversity of Chinese Academy of Sciences, Beijing 100049, China

^cNanjing Institute of Future Energy System, Nanjing 211135, China

^dDepartment of Chemical Engineering, Imperial College London, London SW7 2AZ, UK

^eKey Laboratory of Ocean Energy Utilization and Energy Conservation of Ministry of Education, Dalian, 116024,

China

Corresponding author: gjf1200@126.com (Jiangfeng Guo)

N.B.: This is the accepted version of this article. The final, published version of the article can be found at: <https://doi.org/10.1016/j.applthermaleng.2021.117802>

Abstract

The introducing water mist into the cold channel of recuperator was adopted to improve the thermal-hydraulic performance of compressed humid air in a megawatt grade humid air turbine cycle. The influences of mist content, air pressure and droplet diameter on the thermal-hydraulic performance of the humid air were numerically simulated. The results showed that when the quantity of mist increased from 0 to 16%, the pressure drop decreases by 24.35% while the Colburn factor increases by 8%. The method can effectively mediate the contradiction between heat transfer and resistance. However, the variation of air pressure had little effect on the thermal-hydraulic performance. Besides, the best heat transfer performance can be realized when the inlet droplet diameters are between 5 to 10 μm . A new heat transfer enhancement factor of mist content was proposed, and the correlations of the Nusselt number

and friction factor were obtained. When enhancement factor increases from 0 to 0.16, the Nusselt number increases by 141.5%, and the friction factor decreases by 86.4%. The method of injecting mist can improve the thermal-hydraulic performance and reduce the volume of recuperator, which is further beneficial to reduce the cost and promote the thermal efficiency in the practical application of humid air turbine cycle. It has high application value in the future commercial application of humid air turbine cycle. The results and correlations can provide model and guidance for the design and application of recuperator and humid air turbine cycle.

Keywords: Mist/humid air two-phase; Recuperator; Airfoil; Evaporation; Humid air turbine cycle

1. Introduction

The humid air turbine (HAT) cycle is one of the most representative research directions of the advanced gas turbine cycle. Due to introducing water or steam to turbines, the HAT cycle has the advantages of high power output and low NO_x emissions [1]. Particularly, the recuperator bears the key role of improving the thermal efficiency of the HAT cycle, where waste heat from the exhaust flue gas is used to preheat the compressed humid air. Brighenti et al. [2] found that the recuperator and intercooler are the key components with the largest influence on thermal efficiency and total cost. Therefore, it is necessary to conduct in-depth research on recuperators with high effectiveness and low flow resistance in the HAT cycle, which is significant for the development of HAT cycle power systems.

The working fluids of the recuperator are the wet flue gas and the compressed humid air. Herrmann et al. [3] found that compared with dry air, humid air has higher specific heat and thermal conductivity, lower density and viscosity coefficient, and has better aerodynamic and heat transfer characteristics. Thus, the moisture content of the working fluids has a great effect on the heat transfer characteristics of the recuperator. Many studies have been carried out to extensively research the heat transfer characteristics of humid working fluids flowing in heat exchangers with different inlet air relative humidities and air pressures. Gu et al. [4] experimentally studied the condensation heat transfer characteristics of humid air outside a finned tube and found that the heat transfer

coefficient increases with increasing steam mole fraction. For the influence of air pressure, the heat and mass transfer characteristics of humid working fluids flowing in heat exchangers were discussed under low environmental pressure in the application of high-altitude locations [5-8]. They found that the Colburn factor with heat transfer decreased gradually with decreasing environmental pressure, while the Colburn factor with mass transfer showed a transient rise during the descent process [6]. According to the review of the literatures, humid working fluids are generally at low temperature and atmospheric pressure, and the thermal-hydraulic performances are mainly related to condensing heat transfer in the fields of refrigeration, waste heat recovery, dehumidification and so on. As a result, the heat transfer and flow characteristics of high temperature ($>500\text{ }^{\circ}\text{C}$) and high pressure ($>0.4\text{ MPa}$) humid working fluids flowing in heat exchangers have rarely been investigated.

With the advancement in technology, numerous research institutions [9-11] have successfully established prototype machines of the HAT cycle. However, the electrical output of these prototypes was relatively low ($<150\text{ kW}$), and conventional tube and shell recuperators or plate recuperators were used. As the output power of the HAT cycle expands to the megawatt (MW) scale, a microchannel recuperator with high efficiency and compactness has tremendous application potential. Recently, a microchannel recuperator, built by the Central Research Institute of Electric Power Industry of Japan [12], was applied in a 40 MW HAT cycle.

Nowadays, many high-efficiency and compact microchannel recuperators have been proposed, such as primary-surface recuperators, plate-fin recuperators and printed circuit heat exchangers (PCHE) [13]. PCHEs are extensively used in the supercritical carbon dioxide (S-CO₂) Brayton cycle [14], helium Brayton cycle [15], and supercritical liquefied natural gas-floating production storage and offloading [16]. PCHE has a high-integrity core whose structural strength is the same as the base metal, and it can bear the high-temperature and high-pressure environment of the MW grade HAT cycle. In recent years, PCHEs with various channel structures have been developed, such as straight channels, zigzag channels, S-shaped channels and airfoil channels. The airfoil channels have the best comprehensive performance [17]. Kim et al. [18] numerically examined the thermal-hydraulic

performance of airfoil fins (NACA 0020) with S-CO₂. They found that total heat transfer rate per unit volume of airfoil fins was almost the same with zigzag fins, while the pressure drop was reduced to one-twentieth compared with zigzag fins. Most recently, Wang et al. [19] established a novel structure of PCHE with airfoil channels and straight channels. The results showed that the airfoil fins can significantly increase the heat transfer performance of molten-salt. Fu et al. [20] used the same structure to study the heat transfer characteristics of S-CO₂ and molten-salt. Airfoil fins were designed for S-CO₂ due to the low heat transfer coefficient, and rectangular straight fins were designed for molten-salt owing to the high-pressure loss. Shi et al. [21] numerically investigated the heat transfer characteristics of molten-salt and S-CO₂ in this PCHE under realistic operating conditions (>973 K, 20 MPa) of concentrating solar power. Recently, we [22] numerically simulated the flow and heat transfer performance of compressed humid air and flue gas flowing in this PCHE. The results showed that an increase in moisture content can enhance the heat transfer characteristics for both humid air and wet flue gas. The compressed humid air at the inlet of the recuperator is at a low temperature, the moisture content of humid air at the inlet has an upper limit due to the limitation of saturation temperature and saturation pressure. However, the compressed humid air is heated constantly while it flows in the microchannels, which means that the compressed humid air at the outlet of the recuperator is still unsaturated. In order to increase the moisture content of the outlet, water mist is introduced. The mist-air phase change cooling technique is an important and promising technology for cooling gas turbine blades and heat removal from heat sinks [23]. Many studies have been carried out to research mist-air impinging jet cooling [24], mist-steam convective cooling [25] and mist-air film cooling [26]. Based on the principle of the mist-air phase change cooling technique, the mist can be injected into compressed humid air upstream of the cold microchannel. Then the supersaturated compressed humid air carrying mist is gradually heated in the recuperator, and the moisture content of outlet increases due to mist evaporation. In addition, the heat transfer performance of the recuperator is strengthened because of the phase change heat transfer. As a result, the system comprehensive performance of the HAT cycle is improved. However, the heat transfer behavior of compressed humid air with mist flowing in an airfoil

channel recuperator has hardly been reported in the open literatures. Air pressure also affects the boiling point and evaporation latent heat of mist. The effect of the mist inlet diameter and inlet mist content on the flow and heat transfer characteristics is not clear. Furthermore, relevant heat transfer correlations are deficient, which are vital for the optimization and design of recuperators for HAT cycles.

Thus, the present work developed a numerical study on the flow and heat transfer behavior of mist/compressed humid air two-phase flowing in an airfoil channel recuperator for a HAT cycle. The novel PCHE structure was used, the mist/compressed humid air flowed in a staggered airfoil fin channel, and wet flue gas flowed in a rectangular straight fin channel. Then, the influences of the mass flow rate, air pressure, mist content and mist inlet diameter on the heat transfer and flow characteristics of mist/compressed humid air flowing in the airfoil channel were analyzed. Additionally, the heat transfer correlations were obtained for the mist/compressed humid air. The influence of the mist content on the flow and heat transfer behavior was quantitatively analyzed.

In present study, the method of water mist injection is proposed to further improve the outlet moisture content of humid air, the heat transfer is enhanced through phase transformation, and flow resistance is reduced. The method can effectively mediate the contradiction between heat transfer and resistance of the recuperator in the literature reports. The application of this technology can effectively reduce the system cost and improve the thermal efficiency of the HAT cycle, which plays an important role in the future commercial application of the HAT cycle.

2. Numerical methodology

2.1 Physical model

The novel heat exchanger unit structure combined with an airfoil channel and a straight channel was referred to studies by Wang et al. [19] and Shi et al. [21]. The three-dimensional physical model was demonstrated in [Fig. 1](#). A single rectangle straight channel and a single airfoil channel were chosen as the simulation domain, because the flow was symmetrical and periodic. The NACA 0020 airfoil fins were selected. The inlet boundary condition was the mass-inlet. The outlet was the pressure outlet boundary. The interfaces between fluid region and solid region

were coupled and no-slip boundary. The periodic boundary was set for the top and bottom surface, while the symmetry boundary was set for left and right surface. The adiabatic boundary was set for other surfaces. The geometric dimensions were showed in Table 1.

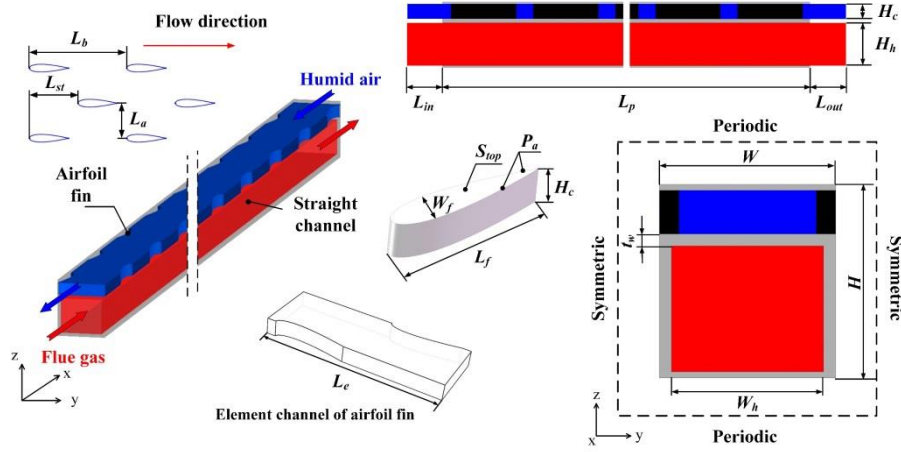


Fig. 1 Schematic diagram of the model

Owing to the limitation of pressure loss in the flue gas side at ordinary pressures, the mass flow rate of hot flue gas cannot be large. The limitation of pressure loss on the flue gas side was set at 2% in the present work, and then the mass flow rate of the wet flue gas changed from $0.5 \times 10^{-5} \text{ kg}\cdot\text{s}^{-1}$ to $1.1 \times 10^{-5} \text{ kg}\cdot\text{s}^{-1}$. The mass flow rate of humid air was 90% of the flue gas mass flow rate [12, 27], which corresponded to $0.45 \times 10^{-5} \text{ kg}\cdot\text{s}^{-1}$ to $0.99 \times 10^{-5} \text{ kg}\cdot\text{s}^{-1}$. The Reynolds numbers ranged from 1000 to 1900.

Table 1 Detailed geometric dimensions

Dimensions	Size/mm	Dimensions	Size/mm
Length L_p	400	Longitudinal pitch L_b	10
Width W	3.6	Transverse pitch L_a	3.6
Height H	4.1	Staggered pitch L_{st}	5
Length of airfoil fin L_f	4	Height of straight fin H_h	2.6
Width of airfoil fin W_f	0.8	Width of straight fin W_h	3.1
Height of airfoil fin H_c	0.9	Height of wall t_w	0.3
L_{in} and L_{out}	10	Length of element L_e	10

Liquid water was selected as the material of the mist. The working pressure had an influence both on the latent heat and boiling point of water. When the pressures of compressed air were 0.4 MPa, 0.7 MPa and 1MPa, the

corresponding boiling points were 416.79 K, 438.15 K and 453.07 K, respectively. The corresponding latent heats were 2133.6 kJ·kg⁻¹, 2066 kJ·kg⁻¹ and 2014.8 kJ·kg⁻¹, respectively. In order to guarantee that the droplet at the outlet of the airfoil channel evaporated completely, the initial diameter of the mist changed from 2 μm to 20 μm, and the mass-flow-rate of the mist changed from 0.386×10⁻⁵ kg·s⁻¹ to 1.416×10⁻⁵ kg·s⁻¹, after the change above, the mist/humid air mass ratios (ω) were 0.08, 0.12 and 0.16, respectively.

2.2 Heat transfer fluids

The components of the wet flue gas were as follows: N₂ 75.6%, O₂ 16.09%, CO₂ 3.04%, and H₂O 5.2% by volume, which can be calculated by the combustion of the natural gas at an excess air coefficient of 4 [28]. The thermophysical properties of flue gas were calculated as follows [29, 30]:

$$\alpha = \sum_{i=1,2,\dots}^n Y_i \alpha_i \quad (1)$$

where Y_i is the mass fraction of different species, i represents species 1, 2, etc., α denotes the density, specific heat at constant pressure, thermal conductivity and viscosity, and n is the amount of the species. The thermal physical properties of different pure gases (N₂, O₂, CO₂ and H₂O) were obtained from NIST data. These physical properties and corresponding mass fractions were substituted into Eq. (1). Then the thermal physical properties of wet flue gas were acquired. The thermal physical properties comparison between the standard exhaust gas [31] and theoretical results was performed in Fig. 2 with the maximum deviation of ±9%. The exactitude of the thermal physical properties' calculation method was verified. The thermal physical properties of flue gas at different temperature were fitted in the form of polynomial functions, which were shown in Table A1.

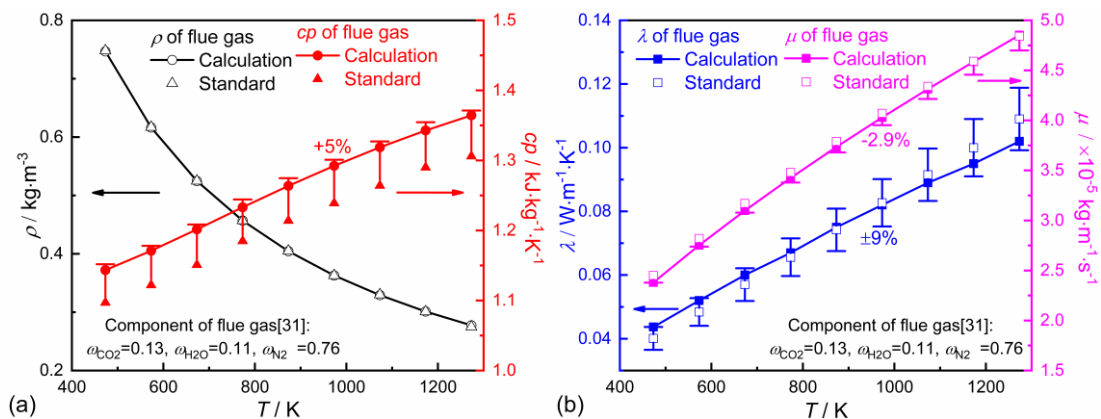


Fig. 2 Thermophysical properties comparison of wet flue gas

In the process of mist-air cooling, the temperature and moisture content of the compressed humid air changed with mist evaporation. The species transport model was used to simulate compressed humid air in the present work. The species of dry air and water vapor were added to this model. In the physical property setting of the species transport model, the ideal gas model was adopted for the density, the mixed law was adopted for the specific heat at constant pressure, and the ideal gas mixed law and mass-weighted mixed law were adopted for the thermal conductivity and dynamic viscosity, respectively. Kinetic theory was used to determine mass diffusivity. The thermal physical properties of dry air and water vapor at different operating pressures and temperatures were fitted by polynomial functions and were given in Table A2 and A3, which were obtained from the NIST data. It should be noted that the temperature of pure water is higher than 443.15 K at a pressure of 0.7 MPa when water is in the gas state. The thermal physical properties of water vapor at low temperature were obtained by the extension of the fitting formulas in Table A3. The calculated thermal physical properties of the compressed humid air under different pressures and moisture contents were compared with the experimental results [32, 33], as shown in Fig. 3, and the maximum deviation was +3.6%. The results demonstrate the accuracy of the transport property calculation models.

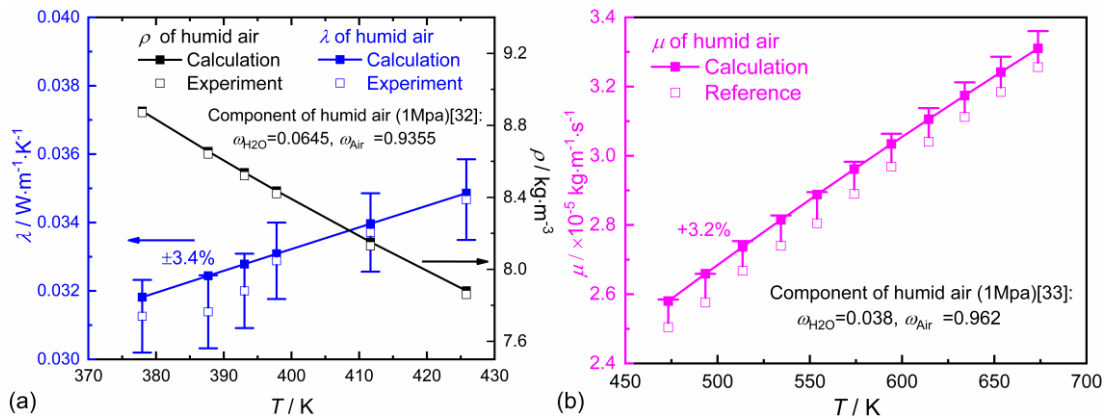


Fig. 3 Thermal physical properties comparison of compressed humid air

The pressure of compressed humid air was 0.4 MPa, 0.7 MPa and 1 MPa, and the inlet temperature was 353.15 K in this study. The compressed humid air with mist at the inlet position was in a supersaturated state, thus the mass fractions of vapor in the saturated humid air were 0.077, 0.043 and 0.03, respectively. The inlet temperature of wet

flue gas was 823.15 K.

The material of solid region is stainless steel 316L, whose thermal conductivity changed with the change in temperature. The thermal conductivity of the solid was also fitted in the form of a polynomial function and given as $\lambda=8.850+0.01565T$.

2.3 Numerical model

The Euler method was employed to perform the continuous phase flow. The Lagrange method was applied to describe the mist droplet phase. The discrete phase model (DPM) was adopted. The three-dimensional governing equations of continuity, momentum and energy were solved combined with the SST $k-\omega$ turbulent model [34]. The reflection boundary condition was set to the wall of the airfoil channel when the droplet impinged on the channel wall, while the heat exchange between the droplet and channel wall was considered [35]. The gravity was considered in the simulation. The governing equations which were based on time-averaged steady-state conditions can be found in Jiang's study [23].

To obtain a stable and reasonable initial field, the convergent flow field and temperature field of the continuous phase were first obtained. Then, the discrete phase was built. The droplets were injected from the inlet of the airfoil channel with the same inlet velocity and temperature as for the continuous phase. The equations and boundary conditions for the continuous phases and discrete phases were solved in an interactive way. The number of continuous phase iterations per DPM iteration was 10. The particle treatment model of unsteady particle tracking was adopted. The particle time step was set to 0.0001, and the number of time steps was 1. Stochastic tracking models of the discrete random walk model and random eddy lifetime were used to describe the droplet turbulent dispersion. The stochastic collision and coalescence of the droplet were considered in the present work. Automated tracking scheme selection, accuracy control tracking options and linearized source terms were adopted to improve the accuracy and stability of the simulation. Moreover, the outlet temperature of compressed air and flue gas and the mass fraction of vapor in the outlet of the airfoil channel acted as monitors in the simulations of flow. When the

changes in these monitor variables were less than 0.1%, the steady-state solution of water droplet evaporation was reached.

The ANSYS FLUENT software was used to conduct the simulation. The SIMPLE algorithm was conducted for coupling of pressure and velocity, and the second-order windward scheme was carried out for the convection and diffusion terms. The convergence was determined when the criteria of continuity, momentum, turbulent kinetic energy and turbulent dissipation were below 1×10^{-5} , and the energy was below 1×10^{-6} .

2.4 Parameter definition

The periodic element channel of airfoil fin was showed in Fig. 1. The calculation methods of the hydraulic diameter (D), convective heat transfer coefficient (h), Reynolds number (Re), Nu , Prandtl number (Pr), Colburn factor (j) and Fanning friction factor (f) can be found in previous studies [19, 21].

The effectiveness of recuperator is obtained by:

$$\varepsilon = \frac{(T_{g,in} - T_{g,out}, T_{a,out} - T_{a,in})_{\max}}{(T_{g,in} - T_{a,in})} \quad (2)$$

where ε is the effectiveness of recuperator, the subscript ‘g’ and ‘a’ indicate the flue gas and humid air, respectively.

The subscript ‘in’ and ‘out’ indicate the inlet and outlet, respectively.

The overall heat transfer coefficient is obtained by:

$$K = \frac{Q}{\Delta T_m AH_a}$$

$$\Delta T_m = \frac{(T_{g,in} - T_{a,in}) - (T_{g,out} - T_{a,out})}{\ln[(T_{g,in} - T_{a,in}) - (T_{g,out} - T_{a,out})]} \quad (3)$$

where K is the overall heat transfer coefficient, ΔT_m is the logarithm mean temperature difference between the flue gas and humid air. AH_a is the heat transfer area of the humid air, which is 0.003 m^2 . Q is the total heat flux containing mist evaporation.

2.5 Mesh and Model validation

The hexahedral meshes were generated by ANSYS ICEM software, as shown in Fig. 4. The specific grid setting can refer to our previous study [34]. The grid independence validation was also carried out, as shown in Fig. 5. The

maximum deviation of outlet temperatures was 0.046K when the mesh numbers were larger than 15,191,200. Thus, a mesh number of 15,191,200 was applied to the current simulation.

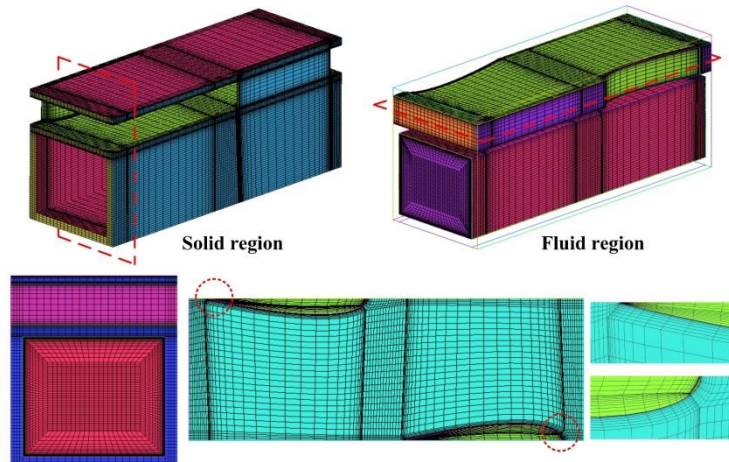


Fig. 4 Meshes of the model

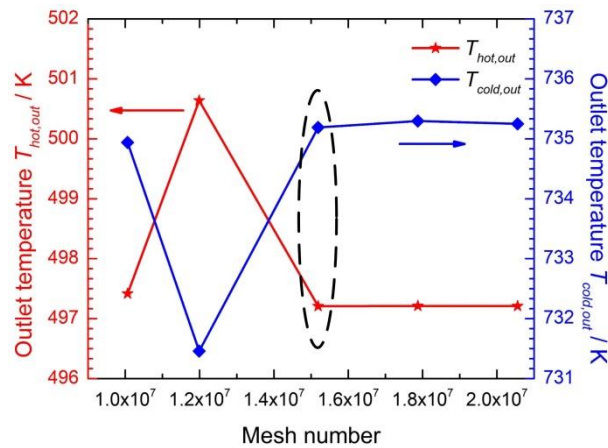


Fig. 5 Variation of outlet temperature with mesh number (case 2, mass-flow-rate of flue gas is $0.0001 \text{ kg}\cdot\text{s}^{-1}$)

Since the experimental results of air flowing in the airfoil channel are deficient, a comparison with Kim's experiments [36] in zigzag channel is performed to confirm simulation reliability. Detailed validations were carried out in our previous work [22].

Furthermore, the heat transfer characteristics of mist evaporation should also be verified. Owing to the lack of experimental data on compressed humid air with water mist flowing in the microchannel, the water mist evaporative cooling model adopted in the present study was verified by evaporative cooling experiments with a water spray system. In the experiment by Sureshkumar et al. [37], the heat and mass transfer process of evaporative cooling of air by a water spray system was investigated. The experiment was carried out in a once-through wind tunnel facility

with a near-uniform air velocity. The cross-section of the wind tunnel was 0.585×0.585 m, and the length was 1.9 m. The spray hollow-cone nozzle was installed in the central position of the inlet cross-section. The velocity probe and two pairs of thermocouples were placed upstream of the nozzle, which measured the inlet velocity, inlet dry bulb temperature (DBT) and wet bulb temperature (WBT), respectively. There were 9 pairs of thermocouples placed at the center of a 3×3 grid in the outlet of the wind tunnel. They were installed in three rows, and each row had three pairs (one for DBT and the other for WBT). According to the experimental system, a three-dimensional computational model was built (Fig. 6(a)). The hexahedral meshes were generated with ANSYS ICEM software. The 1,188,100 hexahedral cells were chosen based on the grid-sensitivity analysis (Fig. 6(b)). The distance from the center point of the first layer grid to the wall was 0.001 m to guarantee that the y^+ value was less than 1. The SST $k-\omega$ turbulent model was adopted. The hollow-cone spray model provided by Fluent was used. The number of particle streams was 300. The droplet size distribution of the Rosin-Rammler model was adopted. The minimum droplet diameter was $74 \mu\text{m}$, the maximum diameter was $518 \mu\text{m}$, the mean diameter was $369 \mu\text{m}$, the spread parameter was 3.67, and the number of diameters was 20. The above parameters were verified in the simulation by Montazeri et al. [35]. The rest of the settings were consistent with the present work, as shown in Section 2.3.

The simulation results (CFD) and the experimental results (EXP) were compared for the three cases in Table 2. The comparison results are shown in Fig. 7, which shows good agreement within a maximum deviation of $\pm 10\%$ for DBT and WBT for all cases. These comparison results showed that the methods and models adopted in this study were correct.

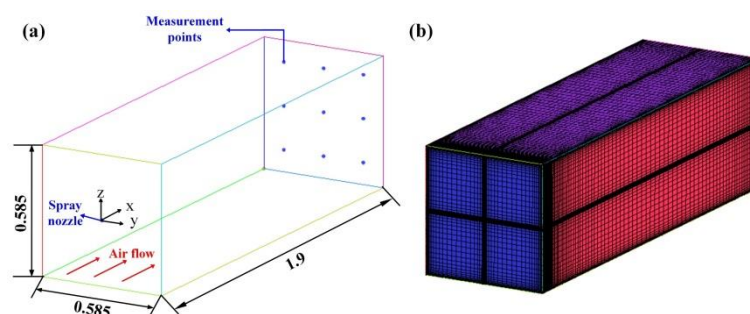


Fig. 6 The computational model (a) geometry (dimensions in meter) (b) grid (1,188,100 cells)

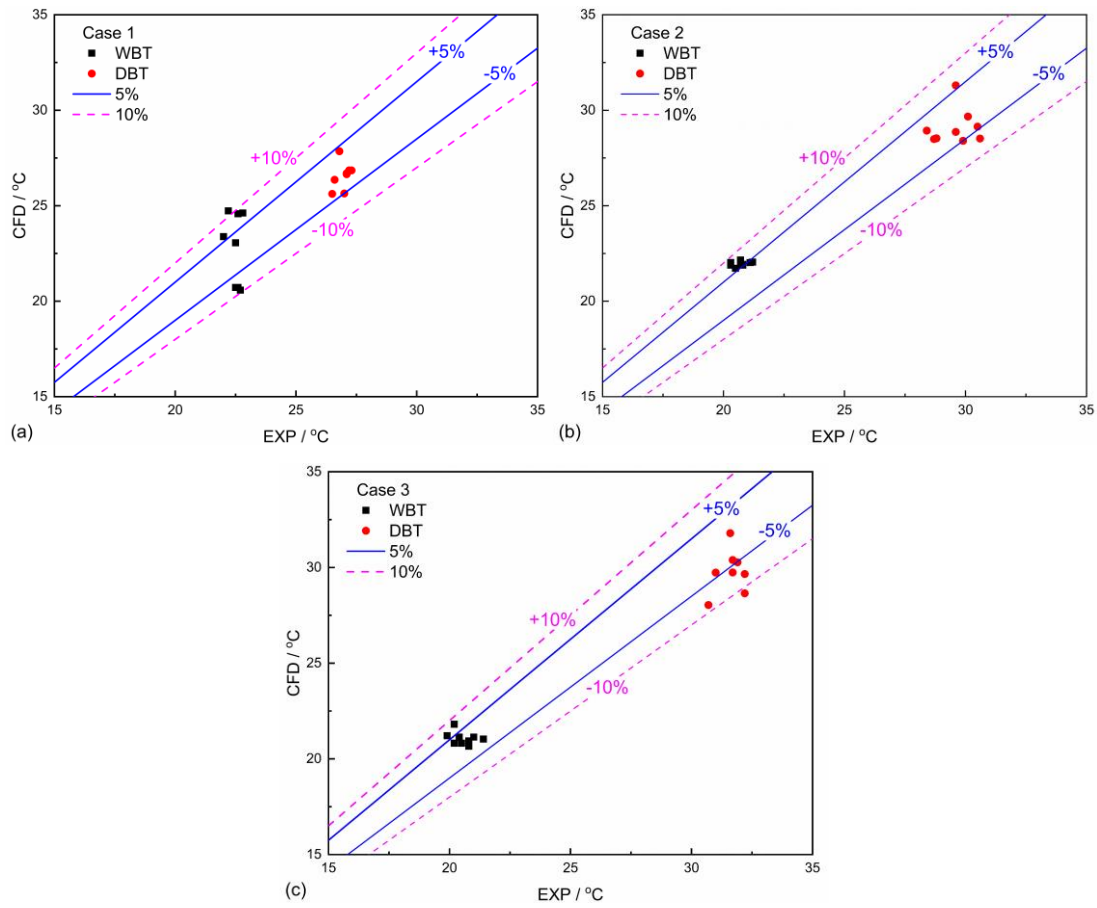


Fig. 7 Comparison of simulation result (CFD) and the experimental result (EXP) of DBT and WBT for case 1, 2 and 3, respectively

Table 2 The parameters of the cases in the experiment

Case	Inlet air				Water				Spray nozzle	
	Velocity ($\text{m}\cdot\text{s}^{-1}$)	DBT ($^{\circ}\text{C}$)	WBT ($^{\circ}\text{C}$)	Mass fraction of vapor	P (bar)	T_{in} ($^{\circ}\text{C}$)	Velocity ($\text{m}\cdot\text{s}^{-1}$)	VF ($\text{lit}\cdot\text{min}^{-1}$)	Diam. (mm)	β (deg.)
1	1	41.4	18.9	0.0046	3	35.1	22	12.5	4	22.0
2	2	39.1	18.5	0.005	3	35.0	22	12.5	4	20.0
3	3	39.2	18.7	0.0052	3	35.2	22	12.5	4	18.0

3. Results and discussions

3.1 Heat transfer and friction characteristics of the airfoil channel

This part is mainly aimed at analyzing the effects of the mass flow rate, pressure and the mist/humid air mass ratio on the j factor and f factor of the airfoil channel. It should be noted that the mist inlet diameter is $10\ \mu\text{m}$ in this part.

The pressure drops and resistance characteristics of the hot and cold channels are important constraint indexes

for the recuperator design. Generally, the total pressure loss should be no more than 5% to satisfy practical applications [38]. The pressure drops of the airfoil channel under different mass flow rates, pressures and ω are shown in Fig. 8. The pressure drop decreases with increasing ω . The pressure drop declines from 2394 Pa to 1811 Pa with the change in ω from 0 to 16% when the pressure is 0.7 MPa and mass flow rate is $8.85 \times 10^{-5} \text{ kg} \cdot \text{s}^{-1}$. This can be explained that the density increases due to the increase in ω , velocity decreases at the same mass flow rate, then the resistance is reduced. The pressure drop decreases with the increase of pressure, and the decreasing amplitude declines gradually. The density increases with increasing pressure, which leads to the velocity decreasing even further. These phenomena indicate that increasing the mist content and pressure can reduce the resistance of cold channels. The temperature distributions of hot and cold channel along the flow direction were shown in Fig. 9. As shown in Fig. 9, due to the heat absorption of evaporation, the heat transfer rate of the hot flue gas increases, and the outlet temperature of the straight channel decreases furtherly. The average temperature of hot flue gas decreases, which leads to velocity decreases, and a reduction in the hot side pressure drop is realized.

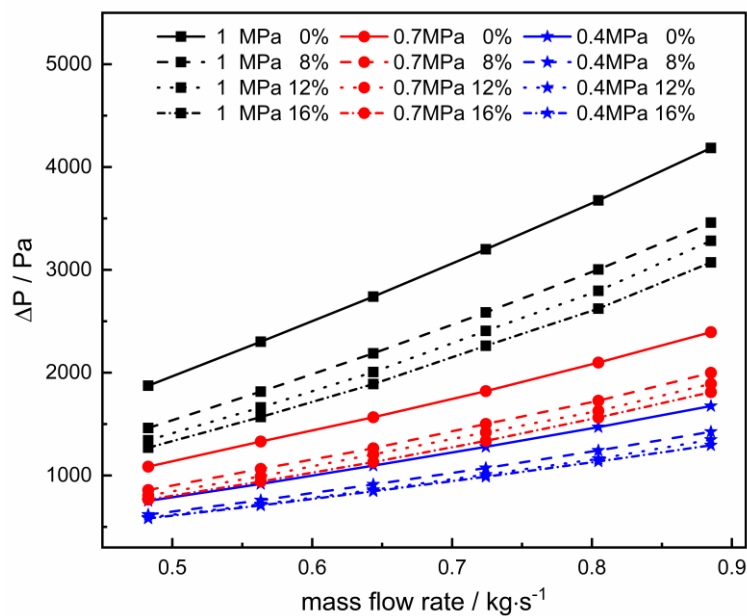


Fig. 8 Pressure drop versus mass flow rate and mist/humid air mass ratio

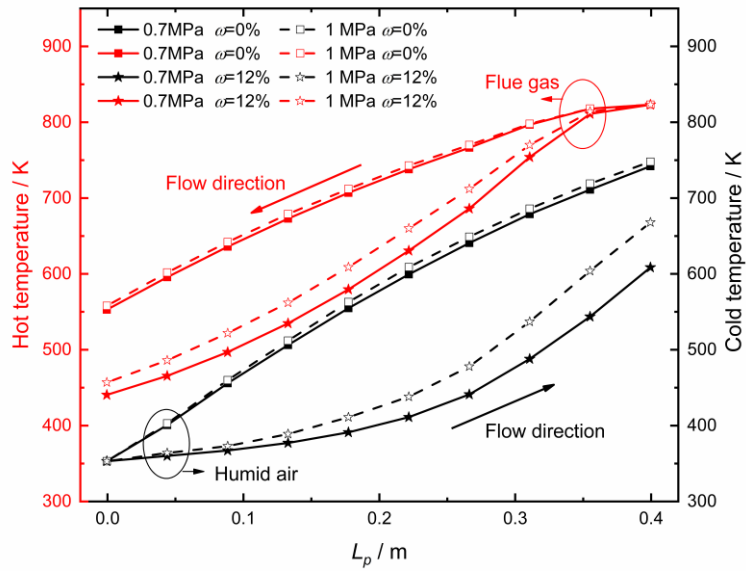


Fig. 9 Temperature distributions of hot and cold channel along the flow direction

The f factors of the airfoil channel under different mass flow rates, pressures and ω are shown in Fig. 10. When ω increases, both the velocity and pressure drop decrease. The decrease in the square of the velocity is larger than pressure drop, leading to a decrease in f . However, the pressure has little effect on f . Although f increases with increasing pressure when ω is constant, the difference is very slight, especially at low mist contents. It can be concluded that injecting mist into the compressed humid air can effectively reduce the resistance of the channel, but increasing pressure has little effect on its reduction. Thus, injecting mist into compressed humid air is an effective method to reduce the resistance of the hot and cold channels of recuperators.

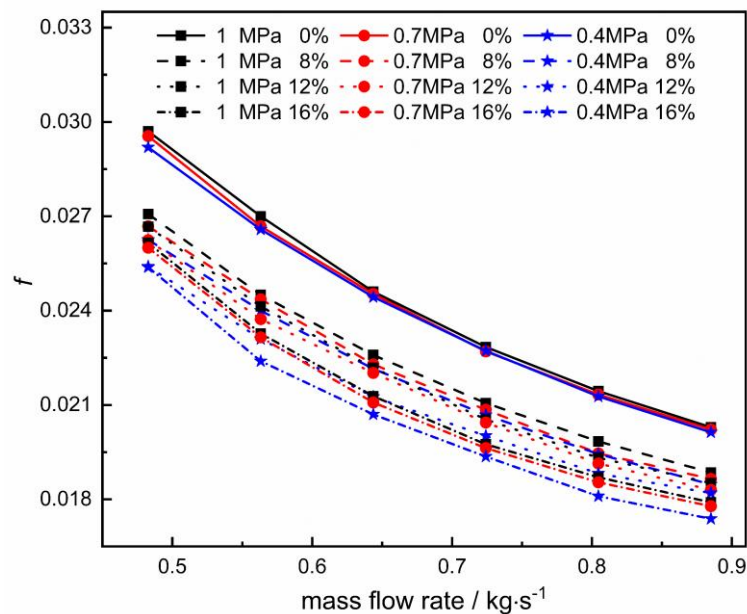


Fig. 10 f factor versus mass flow rate and mist/humid air mass ratio

In addition to the resistance characteristic, the heat transfer characteristic is also an important performance index of the recuperator. The j factors of the airfoil channel under different mass flow rates, pressures and ω are shown in Fig. 11. j decreases with descending ω . A larger ω results in a greater heat transfer rate increase, and Nu increases. However, the increment of Re is very small, which causes the increment of j . Similarly, the pressure also has little effect on j . Although j has a maximum when the pressure is 0.7 MPa, the difference is very slight, especially at high pressure. Consequently, injecting mist into the compressed humid air can effectively improve the heat transfer characteristics of the channel, but increasing pressure has little effect on its improvement. Thus, injecting mist into compressed humid air is an effective method to improve the heat transfer characteristics of the cold channels of recuperator.

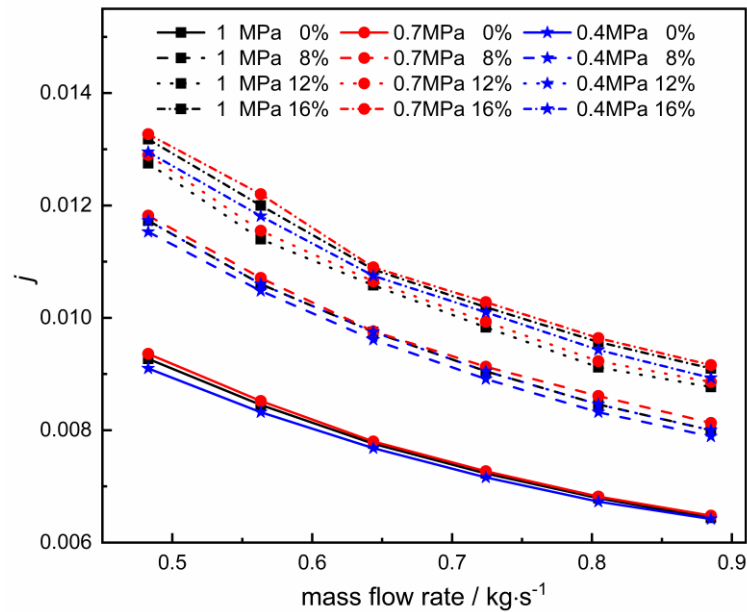


Fig. 11 j factor versus mass flow rate and mist/humid air mass ratio

The comprehensive index $j/f^{1/3}$ is adopted to evaluate the overall performance of different pressures and ω . Fig. 12 displays $j/f^{1/3}$ versus mass flow rate, pressure and ω . $j/f^{1/3}$ increases as ω increases, which means that increasing the mist content can improve the comprehensive thermal-hydraulic performance of cold channels. This is because the heat transfer characteristic is improved while the pressure drop is reduced when mist is injected, which

effectively mediates the contradiction between the heat transfer and resistance characteristic. The pressure has little effect on $j/f^{1/3}$. When the total mass flow rate of inlet work fluids is constant, the comprehensive thermal-hydraulic performance of compressed humid air without mist injection is weaker than that of the compressed humid air with mist injection. In addition, the moisture content of the cold channel outlet can be increased, which is beneficial for improving the thermal-hydraulic performance of cold channels [35]. The inlet moisture content limitation due to the saturation temperature can be broken through by injecting the mist. These characteristics make injecting mist a great potential choice for improving the performance of the recuperator of the HAT cycle.

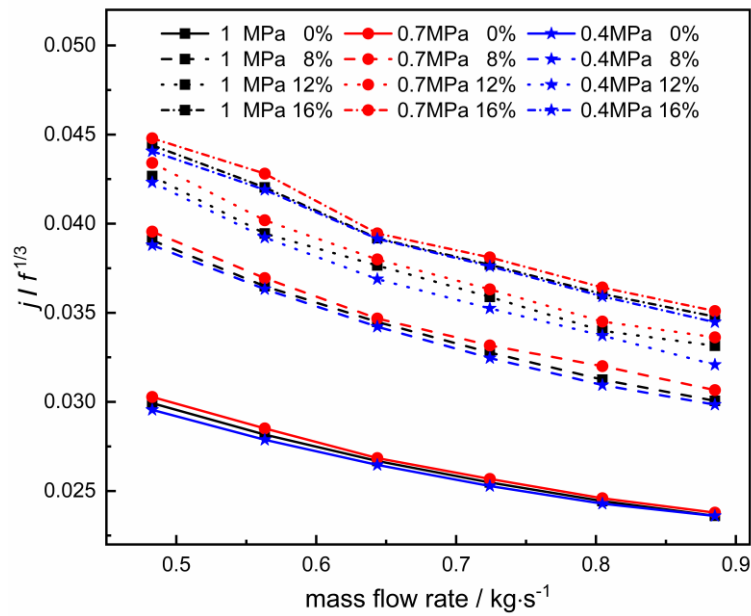


Fig. 12 $j/f^{1/3}$ factor versus mass flow rate and mist/humid air mass ratio

3.2 Performance of the heat exchanger unit

The comprehensive performances of the recuperator, such as the heat transfer effectiveness and the overall heat transfer coefficient, are important performance indexes of the recuperator in practical applications. The mist inlet diameter is also $10\ \mu\text{m}$ in this part.

Fig. 13 depicts the effectiveness versus mass flow rate, pressure and ω . As we can see from Fig. 9, when the mist is injected, the maximum value numerator of Eq. (2) changes from the cold side temperature difference to the hot side temperature difference. The outlet temperature of flue gas increases with the increasing of pressure, which

leads to the effectiveness decreases. When the mist content further increases, the effectiveness gradually increases. This is because the heat transfer rate increases owing to mist evaporation, making the temperature difference between the inlet and outlet of the hot side larger. When there is no mist, the effectiveness increases with increasing pressure, and the increased amplitude decreases gradually. However, when mist is injected, the effectiveness decreases gradually with increasing pressure. After the mist is injected, the evaporation latent heat of the mist with low pressure is high, so the heat absorption of evaporation is greater. This leads to an increase in the heat transfer rate between the flue gas and the humid air. Hence, the outlet temperature of flue gas decreases under countercurrent conditions, and the effectiveness increases. It can be concluded that the pressure and mist content have a great influence on the effectiveness. Notably, the effectiveness can be improved after the mist content reaches a certain threshold value when mist is added. In addition, the effectiveness can be improved by reducing the pressure of the compressed humid air with mist.

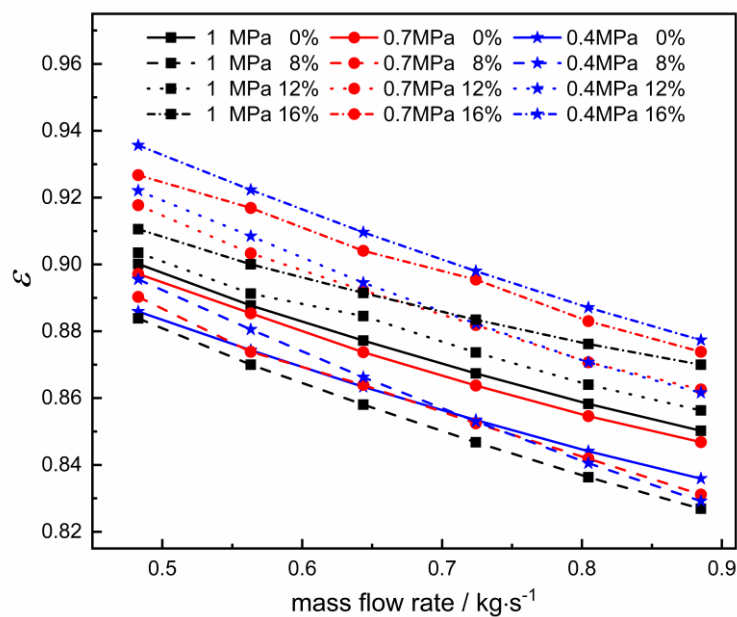


Fig. 13 Effectiveness versus mass flow rate, pressure and mist/humid air mass ratio

Fig. 14 depicts the overall heat transfer coefficient versus mass flow rate, pressure and ω . The coefficients are ranged from $83.5 \text{ W}\cdot\text{m}^{-2}\cdot\text{K}^{-1}$ to $149 \text{ W}\cdot\text{m}^{-2}\cdot\text{K}^{-1}$. The pressure has almost no effect on the overall heat transfer coefficient with no mist injection. When mist is added, the overall heat transfer coefficient gradually increases with

increasing pressure. The ΔT_m is an increasing function with the increase of total temperature difference of hot and cold channel in Eq. (3). The total temperature difference decreases with the increase of pressure in Fig. 9, thus the ΔT_m decreases, resulting in the increase of the overall heat transfer coefficient in Eq. (3). When mist is added, changing the mist content has little effect on the overall heat transfer coefficient. The total heat transfer rate increases with increasing mist content, while the logarithmic mean temperature difference also increases. Combined with Eq. (3), the overall heat transfer coefficient is essentially unchanged.

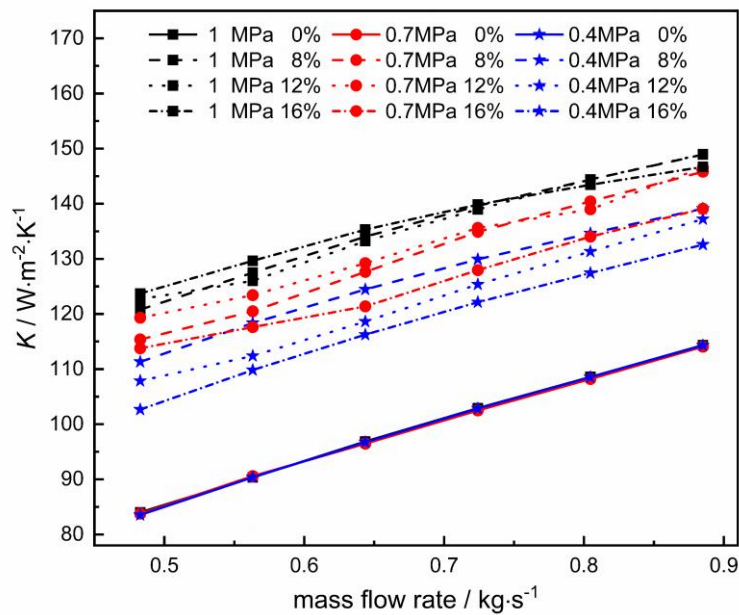


Fig. 14 Overall heat transfer coefficients versus mass flow rate, pressure and mist/humid air mass ratio

3.3 Effect of mist diameter

Mist diameter is the key factor influencing the heat transfer performance of the mist/humid air two-phase flow in the airfoil channel. The mist diameter determines the droplet existence time and evaporation rate [25]. A numerical simulation of different mist inlet diameters (from 2 μm to 20 μm) with different mass flow rates under the condition of 0.7 MPa and $\omega=12\%$ was conducted to study the effect of the inlet mist diameter on the thermal-hydraulic performance.

The curve of Nu versus mist inlet diameter under different mass flow rates (0.7 MPa, $\omega=12\%$) is carried out in Fig. 15. Nu first increases with diameter when the diameter is smaller than 5 μm . Then, Nu basically has no variation.

However, when the diameter is larger than $15\mu\text{m}$, Nu decreases. The reason is that the total mass flux of the mist is a constant value, when the diameter is small, the number of droplets at the inlet position is large. The airfoil channel enhances the mixing of humid air and droplets from the two adjacent fins [21]. Lots of small diameter droplets could coalesce into large diameter droplets driving by the mixing. The evaporation rate reduces due to the increasing of diameter, and large droplets have a long-existing time. Thus, the heat transfer characteristic of humid air is reduced. As the diameter increases, especially for mists whose diameter is larger than $15\mu\text{m}$, there are some droplets that do not evaporate and escape from the outlet. The heat transfer of humid air also reduces. Therefore, it is important to control the mist inlet diameter in the mist cooling technology. Besides, it is seen that as the mass flow rate increases from $4.83\times 10^{-5}\text{ kg}\cdot\text{s}^{-1}$ to $8.85\times 10^{-5}\text{ kg}\cdot\text{s}^{-1}$, the Nu increases around 26.2% when the ω is constant.

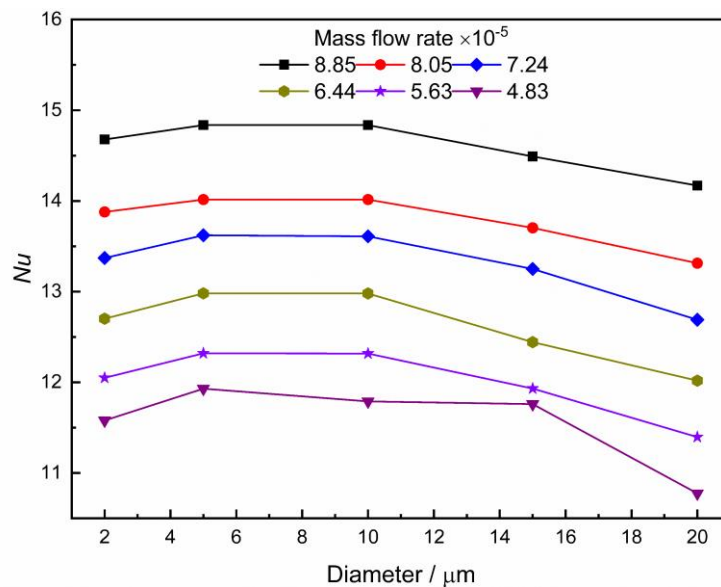


Fig. 15 Nu versus mist inlet diameter under different mass flow rates (0.7 MPa , $\omega=12\%$)

3.4 Correlations of Nu and f for compressed humid air with mist

To direct the optimal design of the recuperator, empirical correlations of thermal-hydraulic characteristics are needed. Moreover, to quantitatively analyze the effect of mist content on flow and heat transfer, the heat transfer enhancement factor of mist content was proposed. The standard properties were selected as variable thermal physical properties of humid air (mist content was 0). Considering the complete evaporation of the mist, the relevant data of inlet diameter of $5\text{-}10\mu\text{m}$ were used in this part. The correlations containing moisture content were fitted as

follows:

$$Nu = 0.704 Re_{in,0}^{0.38} Pr_0^{0.4} \left(1 + \frac{m_{dp}}{m_a}\right)^{2.34} \quad (R^2=0.97) \quad (4)$$

$$f = 2.058 Re_{in,0}^{-0.615} \left(1 + \frac{m_{dp}}{m_a}\right)^{-0.985} \quad (R^2=0.99) \quad (5)$$

where $Re_{in,0}=1000-1900$, $Pr_0=0.75-0.753$, and the subscript '0' indicates that the mist content is 0.

The comparisons of numerical results and fitting results are carried out in Fig. 16. The fitting results match well with the numerical results. The $(1+m_{dp}/m_a)$ in Eqs. (4) and (5) represents the enhanced heat transfer factor. $Re_{in,0}$ and Pr_0 are the inlet Reynold number and Prandtl number of compressed humid air (mist content is 0), respectively. The mist content is the vital factor to influence the flow and heat transfer characteristics of mist/compressed humid air flowing in the airfoil channel. When m_{dp}/m_a is 16%, Nu is improved 141.5% according to Eq. (4), and f is reduced 86.4% according to Eq. (5) when compared with humid air without mist.

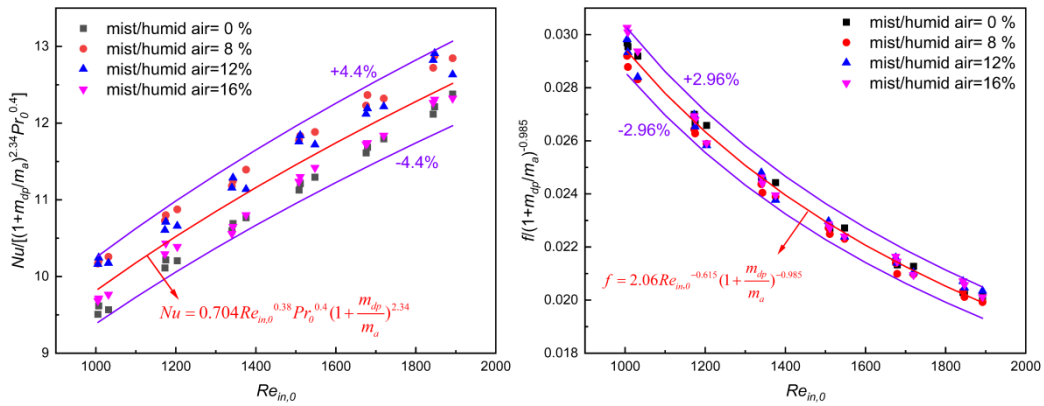


Fig. 16 Nu and f correlations with mist content

4. Conclusions

In this work, the heat transfer characteristics of wet flue gas and compressed humid air with mist in the recuperator unit were numerically simulated. The main conclusions are described below:

- (1) Increasing the mist content and the pressure of humid air can reduce the pressure drop loss of cold airfoil channel. The latent heat of vaporization generated by the evaporation phase transition of water mist leads to the increase of the overall heat transfer. However, pressure increasing has little effect on the heat transfer performance. The results show that the flow and heat transfer characteristics of compressed humid air can be significantly

improved by introducing mist.

(2) When the mist/humid air mass ratio is higher than 8%, increasing the mist content could improve the recuperator effectiveness; however, it almost has no effect on the overall heat transfer coefficient of the recuperator. Increasing the pressure of humid air improves the overall heat transfer coefficient but reduces the recuperator effectiveness. Therefore, in the HAT cycle, it is necessary to select an appropriate pressure and mist content value to balance the comprehensive performance of the recuperator.

(3) An inlet droplet diameter of 5-10 μm can promote the heat transfer performance of compressed humid air with mist.

(4) The correlations of Nusselt number and friction factor of humid air with mist flowing through the airfoil channel are fitted, the heat transfer enhancement factor of mist content is proposed. When enhancement factor increases from 0 to 0.16, Nusselt number increases by approximately 141.5% and friction factor decreases by approximately 86.4%.

The volume of heat exchanger can be reduced under the same heat transfer condition through mist injection, which can effectively reduce the cost and occupation space of heat exchanger in the HAT cycle. The efficiency and economy of the HAT cycle can also be improved. According to the results of this study, the volume of the heat exchanger can be reduced by about one-third when the mist content is 16%, which means it can reduce one-third of the manufacturing cost and occupied space of the heat exchanger. It has economical advantage to the whole system. In conclusion, injecting water mist can significantly improve the flow and heat transfer characteristics of saturated compressed humid air flowing in the airfoil channel. These new correlations and meaningful results can be adopted for the airfoil PCHEs design and performance improvement of the HAT cycle.

Acknowledgements

This work was supported by the National Science and Technology Major Project of China (2017-I-0009-0010), the National Natural Science Foundation of China (52106117) and the Key Laboratory of Ocean Energy Utilization and

Energy Conservation of Ministry of Education.

Appendix. Nomenclature

AH heat transfer area, m^2

D hydraulic diameter, m

f Fanning friction factor

h heat transfer coefficient, $W \cdot m^{-2} \cdot K^{-1}$

H height, mm

H_c height of airfoil fin, mm

H_h height of straight fin, mm

j Colburn factor

K overall heat transfer coefficient, $W \cdot m^{-2} \cdot K^{-1}$

L_a transverse pitch, mm

L_b longitudinal pitch, mm

L_e length of the element, mm

L_f length of airfoil fin, mm

L_{in} length of inlet, mm

L_{out} length of outlet, mm

L_p length, mm

L_{st} staggered pitch, mm

m mass flow rate, $kg \cdot s^{-1}$

Nu Nusselt number

Pr Prandtl number

Q total heat flux with mist evaporation, $W \cdot m^{-2}$

Re Reynolds number

t_w height of wall, mm

T temperature, K

W width, mm

W_f width of airfoil fin, mm

W_h width of straight fin, mm

Y mass fraction of different species

Greek symbols

α density, specific heat at constant pressure, thermal conductivity and viscosity

ΔT_m logarithm mean temperature difference

ΔP pressure drop, Pa

λ thermal conductivity, $W \cdot m^{-2} \cdot K^{-1}$

ε effectiveness of heat exchanger

ω mist/humid air mass ratio

Subscripts

a humid air

dp droplet

g flue gas

i species 1,2,etc

in inlet

out outlet

Abbreviations

CFD	Simulation results
DBT	Dry bulb temperature
DPM	Discrete phase model
EXP	Experimental results
HAT	Humid air turbine
MW	Megawatt
PCHE	Printed circuit heat exchangers
S-CO ₂	Supercritical carbon dioxide
WBT	Wet bulb temperature

Appendix A

Table A1 Thermal physical properties of flue gas

Properties	Polynomial functions of the properties (353 K<T<823 K)
Density	$\rho=2.427-0.006T + 6.54E - 6T^2 -2.56E - 9T^3$
Specific heat	$cp=1119.66-0.53T+1.13E - 3T^2 -5.27E - 7T^3$
Thermal conductivity	$\lambda=0.00343 + 7.83E - 5T -1.43E - 8T^2$
Viscosity	$\mu=4.2E - 6 + 5.05E - 8T -1.22E - 11T^2$

Table A2 Thermal physical properties of dry air

Case	Pressure (MPa)	Polynomial functions of the properties (353 K<T<823 K)
1	0.4	$\rho=7.748-0.0138T + 7.891E - 6T^2$ $cp=983.927+0.0194T + 1.571E - 4T^2$

		$\lambda=0.01+5.826E-5T$
		$\mu=4.247E-6+5.292E-8T-1.424E-11T^2$
		$\rho=12.142-0.0198T+1.052E-5T^2$
		$cp=963.342+0.0886T+1.032E-4T^2$
2	0.7	$\lambda=0.0112+5.668E-5T$
		$\mu=4.995E-6+5.07E-8T-1.26E-11T^2$
		$\rho=19.392-0.0346T+1.984E-5T^2$
		$cp=1001.871-0.0247T+1.859E-4T^2$
3	1	$\lambda=0.0103+5.803E-5T$
		$\mu=4.412E-6+5.26E-8T-1.405E-11T^2$

Table A3 Thermal physical properties of water vapor

Case	Pressure (MPa)	Polynomial functions of the properties (443 K<T<823 K)
		$\rho=6.6832-0.01797T+2.0533E-5T^2-8.5179E-9T^3$
1	0.4	$cp=11605.472-55.598T+0.1197T^2-1.1354E-4T^3+4.0381E-8T^4$
		$\lambda=0.00831+2.313E-5T+6.846E-8T^2$
		$\mu=-3.536E-6+4.153E-8T$
		$\rho=12.9574-0.0367T+4.338E-5T^2-1.843E-8T^3$
2	0.7	$cp=18788.759-95.398T+0.203T^2-1.918E-4T^3+6.796E-8T^4$
		$\lambda=0.0174-1.565E-6T+8.552E-8T^2$
		$\mu=-3.825E-6+4.193E-8T$
		$\rho=19.9144-0.05787T+6.8937E-5T^2-2.9306E-8T^3$
3	1	$cp=31925.199-169.7761T+0.3613T^2-3.4081E-4T^3+1.2044E-7T^4$
		$\lambda=0.0246-1.9621E-5T+9.712E-8T^2$

$$\mu = -4.0042E - 6 + 4.2168E - 8T$$

References

- [1] M. Jonsson, J.Y. Yan, Humidified gas turbines - a review of proposed and implemented cycles, *Energy*, 30(7) (2005) 1013-1078. <https://doi.org/10.1016/j.energy.2004.08.005>.
- [2] G.D. Brighenti, P.L. Orts-Gonzalez, L. Sanchez-de-Leon, P.K. Zachos, Design point performance and optimization of humid air turbine power plants, *Applied Sciences*, 7(4) (2017) 413. <https://doi.org/10.3390/app7040413>.
- [3] S. Herrmann, H.J. Kretschmar, D.P. Gatley, Thermodynamic properties of real moist air, dry air, steam, water, and ice (RP-1485), *HVAC&R Research*, 15(5) (2009) 961-986. <https://doi.org/10.1080/10789669.2009.10390874>.
- [4] Y.H. Gu, Q. Liao, M. Cheng, Y.D. Ding, X. Zhu, Condensation heat transfer characteristics of moist air outside a three-dimensional finned tube, *International Journal of Heat and Mass Transfer*, 158 (2020) 119983. <https://doi.org/10.1016/j.ijheatmasstransfer.2020.119983>.
- [5] B. Kundu, K.S. Lee, Effects of psychrometric properties on fin performances of minimum envelope shape of wet fins, *Energy Conversion and Management*, 110 (2016) 481-493. <https://doi.org/10.1016/j.enconman.2015.09.054>.
- [6] Q. Liu, J.H. Liu, L. Zhang, X.J. Xu, Effect of environmental pressure on heat and mass transfer characteristics for fin-and-tube heat exchangers under non-unit Lewis factor, *Applied Thermal Engineering*, 116 (2017) 784-791. <https://doi.org/10.1016/j.applthermaleng.2017.01.093>.
- [7] R.Z. Jia, Y.C. Wang, J. Guo, Z.Y. Yu, H.F. Kang, Research on the heat transfer and flow characteristics of fin-tube exchanger under low pressure environment, *Applied Thermal Engineering*, 112 (2017) 1163-1171. <https://doi.org/10.1016/j.applthermaleng.2016.06.137>.
- [8] M.H. Sharqawy, S.M. Zubair, Efficiency and optimization of an annular fin with combined heat and mass transfer

- an analytical solution, *International Journal of Refrigeration*, 30(5) (2007) 751-757.
<https://doi.org/10.1016/j.ijrefrig.2006.12.008>.
- [9] M. Thern, T.R. Lindquist, T. Torisson, Theoretical and experimental evaluation of a plate heat exchanger aftercooler in an evaporative gas turbine cycle, in: *ASME Turbo Expo 2003, collocated with the 2003 International Joint Power Generation Conference, 2003*, pp. 103-111.
- [10] S. Nakano, T. Kishibe, H. Araki, M. Yagi, K. Tsubouchi, M. Ichinose, Y. Hayasaka, M. Sasaki, T. Inoue, K. Yamaguchi, H. Shiraiwa, Development of a 150kW microturbine system which applies the humid air turbine cycle, in: *ASME Turbo Expo 2007: Power for Land, Sea, and Air, 2007*, pp. 1041-1048.
- [11] Z. Xu, Y. Lu, B. Wang, L.F. Zhao, C.N. Chen, Y.H. Xiao, Experimental evaluation of 100 kW grade micro humid air turbine cycles converted from a microturbine, *Energy*, 175 (2019) 687-693.
<https://doi.org/10.1016/j.energy.2019.03.036>.
- [12] T. Takeda, H. Araki, Y. Iwai, T. Morisaki, K. Sato, Test results of 40MW-class advanced humid air turbine and exhaust gas water recovery system, in: *ASME Turbo Expo 2014: Turbine Technical Conference and Exposition, 2014*.
- [13] G. Xiao, T.F. Yang, H.L. Liu, D. Ni, M.L. Ferrari, M.C. Li, Z.Y. Luo, K.F. Cen, M.J. Ni, Recuperators for micro gas turbines: a review, *Applied Energy*, 197 (2017) 83-99. <https://doi.org/10.1016/j.apenergy.2017.03.095>.
- [14] J.W. Lao, Q.M. Fu, W.L. Wang, J. Ding, J.F. Lu, Heat transfer characteristics of printed circuit heat exchanger with supercritical carbon dioxide and molten salt, *Journal of Thermal Science*, 30 (2021) 880-891.
<https://doi.org/10.1007/s11630-020-1374-3>.
- [15] I.H. Kim, X. Sun, CFD study and PCHE design for secondary heat exchangers with FLiNaK-Helium for SmAHTR, *Nuclear Engineering and Design*, 270 (2014) 325-333. <https://doi.org/10.1016/j.nucengdes.2014.02.003>.
- [16] L.H. Tang, Z. Cao, J. Pan, Investigation on the thermal-hydraulic performance in a PCHE with airfoil fins for supercritical LNG near the pseudo-critical temperature under the rolling condition, *Applied Thermal Engineering*,

175 (2020) 115404. <https://doi.org/10.1016/j.applthermaleng.2020.115404>.

[17] S.H. Yoon, H.C. No, G.B. Kang, Assessment of straight, zigzag, S-shape, and airfoil PCHEs for intermediate heat exchangers of HTGRs and SFRs, *Nuclear Engineering and Design*, 270 (2014) 334-343. <https://doi.org/10.1016/j.nucengdes.2014.01.006>.

[18] D.E. Kim, M.H. Kim, J.E. Cha, S.O. Kim, Numerical investigation on thermal-hydraulic performance of new printed circuit heat exchanger model, *Nuclear Engineering and Design*, 238 (2008) 3269-3276. <https://doi.org/10.1016/j.nucengdes.2008.08.002>.

[19] W.Q. Wang, Y. Qiu, Y.L. He, H.Y. Shi, Experimental study on the heat transfer performance of a molten-salt printed circuit heat exchanger with airfoil fins for concentrating solar power, *International Journal of Heat and Mass Transfer*, 135 (2019) 837-846. <https://doi.org/10.1016/j.ijheatmasstransfer.2019.02.012>.

[20] Q.M. Fu, J. Ding, J.W. Lao, W.L. Wang, J.F. Lu, Thermal-hydraulic performance of printed circuit heat exchanger with supercritical carbon dioxide airfoil fin passage and molten salt straight passage, *Applied Energy*, 247 (2019) 594-604. <https://doi.org/10.1016/j.apenergy.2019.04.049>.

[21] H.Y. Shi, M.J. Li, W.Q. Wang, Y. Qiu, W.Q. Tao, Heat transfer and friction of molten salt and supercritical CO₂ flowing in an airfoil channel of a printed circuit heat exchanger, *International Journal of Heat and Mass Transfer*, 150 (2020) 119006. <https://doi.org/10.1016/j.ijheatmasstransfer.2019.119006>.

[22] J.L. Chen, J.F. Guo, X.F. Li, X.L. Huai, K.Y. Cheng, H.Y. Zhang, Z.X. Han, Thermal-hydraulic performance of compressed humid air flowing in a recuperator, *Applied Thermal Engineering*, 188 (2021) 116620. <https://doi.org/10.1016/j.applthermaleng.2021.116620>.

[23] Y.T. Jiang, Q. Zheng, P. Dong, J.H. Yao, H. Zhang, J. Gao, Conjugate heat transfer analysis of leading edge and downstream mist-air film cooling on turbine vane, *International Journal of Heat and Mass Transfer*, 90 (2015) 613-626. <https://doi.org/10.1016/j.ijheatmasstransfer.2015.07.005>.

[24] A.K. Sharma, S.K. Sahu, An experimental study on heat transfer and rewetting behavior of hot horizontal

- downward facing hot surface by mist jet impingement, *Applied Thermal Engineering*, 151 (2019) 459-474.
<https://doi.org/10.1016/j.applthermaleng.2019.02.038>.
- [25] G.W. Jiang, J.M. Gao, X.J. Shi, F.J. Li, L. Xu, Flow and heat transfer characteristics of the mist/steam two-phase flow cooling the rectangular channel with column-row-ribs, *International Journal of Heat and Mass Transfer*, 156 (2020) 119737. <https://doi.org/10.1016/j.ijheatmasstransfer.2020.119737>.
- [26] A.Q. Lin, Y.G. Sun, H. Zhang, X. Lin, L. Yang, Q. Zheng, Fluctuating characteristics of air-mist mixture flow with conjugate wall-film motion in a compressor of gas turbine, *Applied Thermal Engineering*, 142 (2018) 779-792.
<https://doi.org/10.1016/j.applthermaleng.2018.07.076>.
- [27] W.X. Xi, J. Cai, X.L. Huai, Numerical investigation on fluid-solid coupled heat transfer with variable properties in cross-wavy channels using half-wall thickness multi-periodic boundary conditions, *International Journal of Heat and Mass Transfer*, 122 (2018) 1040-1052. <https://doi.org/10.1016/j.ijheatmasstransfer.2018.02.055>.
- [28] C.Y. Wei, Performance simulation and experimental investigation of a humid air turbine cycle, Shanghai Jiao Tong University, 2014.
- [29] M. Punetha, S. Khandekar, A CFD based modelling approach for predicting steam condensation in the presence of non-condensable gases, *Nuclear Engineering and Design*, 324 (2017) 280-296.
<https://doi.org/10.1016/j.nucengdes.2017.09.007>.
- [30] S. Herrmann, H.J. Kretzschmar, V. Teske, E. Vogel, P. Ulbig, R. Span, D.P. Gatley, Properties of humid air for calculating power cycles, *Journal of Engineering for Gas Turbines and Power*, 132(9) (2010) 093001.
<https://doi.org/10.1115/1.4000611>.
- [31] L. Xu, J.Q. Yuan, Thermodynamic properties calculation of the flue gas based on its composition estimation for coal-fired power plants, *Applied Thermal Engineering*, 90 (2015) 366-375.
<https://doi.org/10.1016/j.applthermaleng.2015.07.018>.
- [32] S.G.S. Beirão, A.P.C. Ribeiro, M.J.V. Lourenço, F.J.V. Santos, C.A. Nieto de Castro, Thermal conductivity of

humid air, *International Journal of Thermophysics*, 33(8) (2012) 1686-1703. <https://doi.org/10.1007/s10765-012-1254-5>.

[33] Y. Peng, S.H. Li, H. Ming, W.X. Cui, L.W. Wang, Y.M. Mo, S. Ma, W.W. Ma, L.Q. Li, Research of properties of humid air at high temperature and high pressure, *Building Energy & Environment*, 7(39) (2017) 22-26.

[34] T. Ma, L. Li, X.Y. Xu, Y.T. Chen, Q.W. Wang, Study on local thermal-hydraulic performance and optimization of zigzag-type printed circuit heat exchanger at high temperature, *Energy Conversion and Management*, 104 (2015) 55-66. <https://doi.org/10.1016/j.enconman.2015.03.016>.

[35] H. Montazeri, B. Blocken, J.L.M. Hensen, Evaporative cooling by water spray systems: CFD simulation, experimental validation and sensitivity analysis, *Building and Environment*, 83 (2015) 129-141. <https://doi.org/10.1016/j.buildenv.2014.03.022>.

[36] I.H. Kim, Thermal hydraulic performance of the printed circuit heat exchanger in air and helium test loops, Korea Advanced Institute of Science and Technology (2008).

[37] R. Sureshkumar, S.R. Kale, P.L. Dhar, Heat and mass transfer processes between a water spray and ambient air - I. experimental data, *Applied Thermal Engineering*, 28(5) (2008) 349-360. <https://doi.org/10.1016/j.applthermaleng.2007.09.010>.

[38] C.F. McDonald, Low-cost compact primary surface recuperator concept for microturbines, *Applied Thermal Engineering*, 20 (2000) 471-497. [https://doi.org/10.1016/S1359-4311\(99\)00033-2](https://doi.org/10.1016/S1359-4311(99)00033-2).